Noble Metal Loaded TiO_2 for Photocatalytic H_2O_2 Production

Meshal Al Johani, Zhirun Xie, Yun Hau Ng

meshal.ab.aljohani@gmail.com

Abstract

Hydrogen peroxide is a strong oxidant and a promising liquid energy carrier, easier to store and move than hydrogen gas, and useful in fuel cells and water treatment. Industry makes it by the anthraquinone process, which takes several steps, uses much energy and produces considerable waste. Photocatalysis offers a direct route: a semiconductor catalyst builds hydrogen peroxide from oxygen and water under light. Two problems limit the yield. The two-electron oxygen reduction reaction competes with the favoured four-electron path to water, and the product decomposes on the surface that formed it. This study identifies which noble metal co-catalyst best promotes production on titanium dioxide, and determines what limits the rate. We deposited gold, silver and platinum onto anatase titanium dioxide at 1 wt% loading, then tested each in a batch photoreactor for four hours under two oxygen regimes: a fixed inventory set by pre-purging, and continuous purging. Hydrogen peroxide was measured by iodometric assay at 350 nm, and the catalysts characterised by X-ray diffraction, scanning electron microscopy and diffuse reflectance spectroscopy. All three metals beat unmodified titanium dioxide, gold by the widest margin. In the first hour gold reaches 228 mM h^{-1} g^{-1} under continuous purging against 6 for the bare oxide. Loading left the anatase structure, crystallite size and band gap unchanged, while plasmon bands confirmed metallic silver and gold. Gold gained 41 per cent from extra oxygen against 79 per cent for platinum and 200 per cent for the bare oxide, so oxygen supply rather than charge separation limits the weaker catalysts.

Date: August 9, 2026

Laboratory: CAREY Lab, Catalysis for Alternative and Renewable Energy

Affiliation: Clean Energy Research Platform, Physical Sciences and Engineering Division, KAUST

Contents

1 Introduction 3
2 Related Work 3
3 Methodology 4
3.1 Method details 4
3.2 Evaluation Procedure 6
4 Results 6
5 Discussion 9
6 Limitations and Future Work 10
7 Conclusion 10
References 10

1 Introduction

Hydrogen peroxide is one of the most widely used oxidants in industry. It bleaches pulp and textiles, disinfects surfaces and water, and treats effluent. Because it breaks down to water and oxygen alone, it leaves no residue where chlorine based oxidants would. It also works as a liquid energy carrier: a fuel cell running on H_2O_2 avoids the storage problems of gaseous hydrogen, since the peroxide is liquid at ambient conditions and needs no cryogenic or high pressure tank.

Almost all commercial peroxide comes from anthraquinone auto-oxidation. An alkyl anthraquinone is hydrogenated over palladium, the hydroquinone is oxidised in air to release H_2O_2, and the product is extracted and concentrated. The route works well but uses large amounts of energy, needs several sequential operations around a recirculating organic solution, and produces waste as that solution degrades.

Photocatalysis works differently [1]. A semiconductor absorbs light above its band gap and generates an electron in the conduction band and a hole in the valence band. If the electron is reducing enough it drives the reduction of oxygen, and if that reduction takes two electrons rather than four the product is peroxide rather than water. A catalyst, oxygen, water and light are therefore enough to make H_2O_2 at ambient conditions [3].

Two things limit the rate. Reduction to water is thermodynamically favoured, so an unmodified catalyst makes water in preference to peroxide. The peroxide it does make is then decomposed on the surface that produced it, and what you measure is formation minus loss. A noble metal on the surface addresses both. Its work function exceeds the electron affinity of the oxide, so conduction band electrons move into the metal and stay there, away from the holes. Recombination falls and the reducing electrons gather at one site. Which metal it is decides which path that site favours, and whether it also destroys the product.

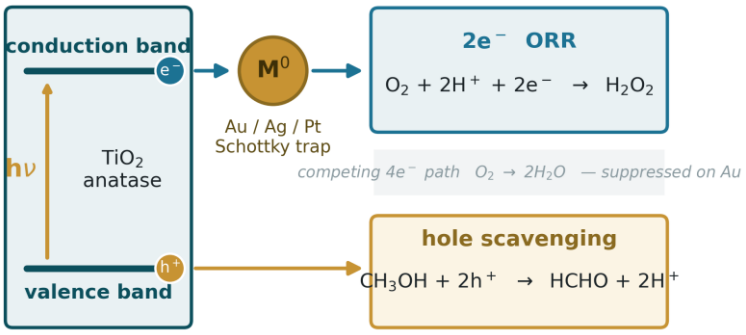


Figure 1 Charge separation at a metal/TiO_2 Schottky junction and the two-electron oxygen reduction route to H_2O_2, with methanol as the sacrificial hole donor.

This project establishes which noble metal co-catalyst best promotes photocatalytic peroxide production on one well defined support, and identifies what limits the rate. Gold, silver and platinum go onto the same batch of anatase TiO_2, at the same loading, by the same method, so any difference reflects the metal and not the preparation. Each catalyst is then tested under a fixed oxygen inventory and under continuous supply, which separates the electronic effect of the co-catalyst from the effect of how much oxygen reaches the surface.

Two assumptions bound the work. Methanol is the sacrificial hole donor throughout, so the system is a reduction half-reaction rather than overall water splitting, and solar to chemical efficiency does not apply. The metal loading is nominal at 1 wt% and has not been confirmed by elemental analysis.

2 Related Work

Photocatalysis on semiconductor electrodes dates to the water splitting work of Fujishima and Honda [1], and titanium dioxide has been the reference material for the chemistry since [8]. Peroxide formation over irradiated titanium dioxide suspensions was reported by Kormann and co-workers in 1988 [9], who measured micromolar yields from TiO_2, ZnO and desert sand.

Selectivity towards the two-electron route, rather than raw activity, is what later work has improved. Shiraishi and co-workers raised it substantially on graphitic carbon nitride by tailoring the surface chemistry [10], and recent reviews cover the range of catalyst systems and the mechanisms behind them [3]. Campos-Martin and co-workers set out the case against the incumbent anthraquinone process in detail [2].

What that literature leaves open is the question this project addresses. Comparisons between co-catalysts are usually run under one set of oxygen conditions, so an improvement attributed to better charge separation may in fact reflect nothing more than how quickly each catalyst consumes the oxygen available to it. Testing the same series under two oxygen regimes separates the two.

3 Methodology

3.1 Method details

The three loaded catalysts were made by photodeposition onto 200 mg batches of anatase TiO_2 at 1 wt% nominal loading. Each metal precursor was dissolved in an aqueous methanol suspension of the oxide, purged with nitrogen, and irradiated. Photogenerated electrons reduce the metal ion to M^0 at the surface while methanol consumes the holes.

Table 1 Precursors and nominal loadings for photodeposition onto 200 mg TiO_2 batches.

Metal	Precursor	Nominal loading
Gold	$HAuCl_4 \cdot 3H_2O$	1 wt%
Silver	$AgNO_3$	1 wt%
Platinum	$H_2PtCl_6 \cdot 6H_2O$	1 wt%

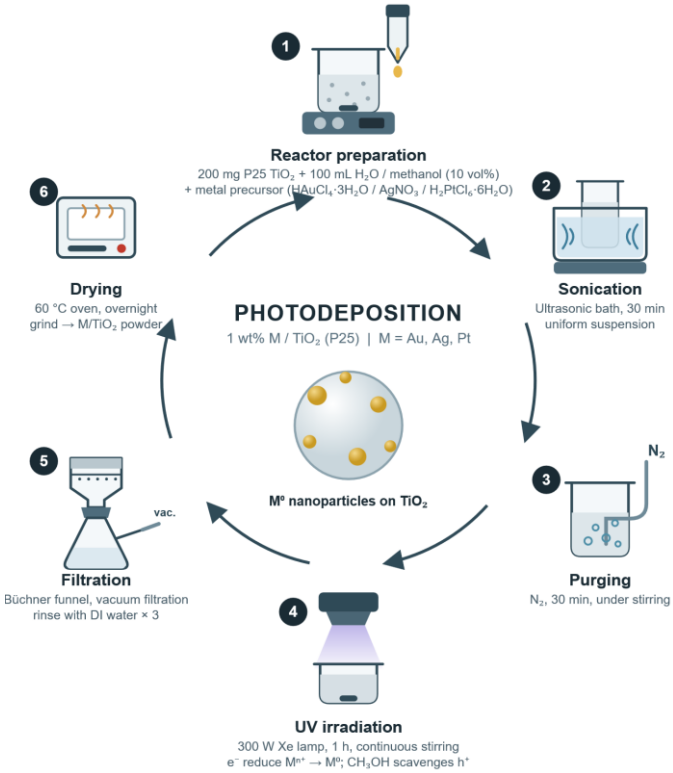


Figure 2 Photodeposition route: reactor preparation, sonication, nitrogen purging, UV irradiation, filtration and drying. The product is 1 wt% M/TiO_2 with M = Au, Ag or Pt.

Reactions ran in a batch photoreactor with the suspension stirred under the illuminated window. Each used 10 mg of catalyst in 25 mL of solution with 10 vol% methanol as sacrificial hole donor. Methanol consumes the holes irreversibly and stops them oxidising the product, isolating the reduction half-reaction. Rates are therefore given as concentration per hour per gram.

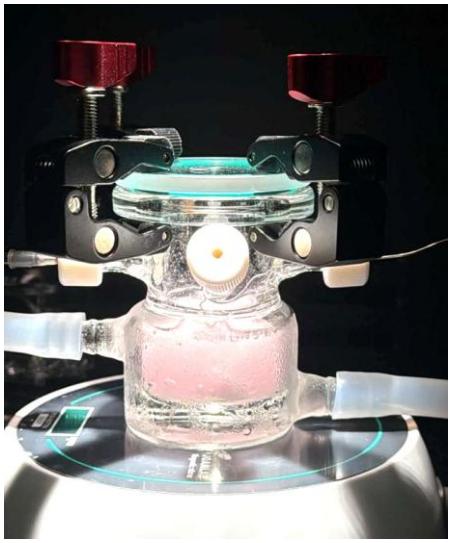


Figure 3 Batch photoreactor under illumination. The rose colouration of the suspension comes from the gold surface plasmon band.

Each run was irradiated for four hours with samples taken hourly. Two oxygen regimes were applied to every catalyst. Under Regime A the suspension was pre-purged with oxygen at 100 mL per minute for 30 minutes and then left, so the dissolved inventory was fixed at the start. In Regime B oxygen flowed continuously at 50 mL per minute. The comparison isolates oxygen mass transport: a catalyst limited by photochemistry behaves alike under both regimes, whereas one that improves under continuous purging was starved of oxygen under the fixed inventory.

3.2 Evaluation Procedure

Peroxide was measured colorimetrically by the iodometric method. Hydrogen peroxide oxidises iodide to triiodide with potassium hydrogen phthalate as buffer, and the triiodide absorbance at 350 nm gives the concentration. The reaction is $H_2O_2 + 3I^- + 2H^+ \rightarrow I_3^- + 2H_2O$.

For each sample, 50 µL of reaction solution was diluted with 950 µL of deionised water, a twentyfold dilution. Then 1 mL of potassium iodide solution and 1 mL of potassium hydrogen phthalate solution were added, for 3 mL in total. The mixed solution was left to stand for 30 minutes at room temperature before the absorbance was read. Standards were prepared by dilution from commercial hydrogen peroxide of 9.8 N concentration and went through the same reagent addition, so the twentyfold pre-dilution is the only factor applied.

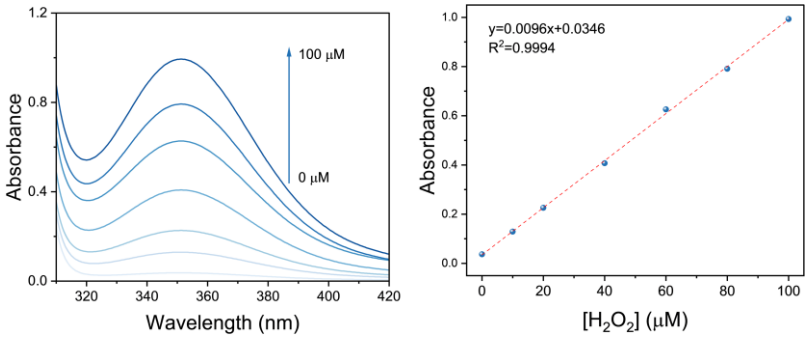


Figure 4 Left: absorbance spectra of the triiodide complex across the calibration range 0 to 100 µM H_2O_2. The band at 350 nm is the one used for quantification. Right: calibration of absorbance at 350 nm against hydrogen peroxide concentration.

The calibration spans 0 to 100 µM and is linear across that range. With the twentyfold dilution the top standard corresponds to 2000 µM in the reaction solution, which is the ceiling the assay can read without extrapolating.

Three techniques were used on every sample. Diffraction identifies the phase, measures the crystallite size and would reveal any bulk metal phase. Microscopy shows what the particles look like. From the optical absorption, reflectance spectroscopy yields the band gap and any sign of metallic nanoparticles. Bare TiO_2 is the baseline against which every loaded catalyst is judged.

4 Results

Patterns were recorded with Cu Kα radiation at 1.5406 Å from 10° to 80° 2θ in 0.0197° steps, all four samples in one session with the same settings.

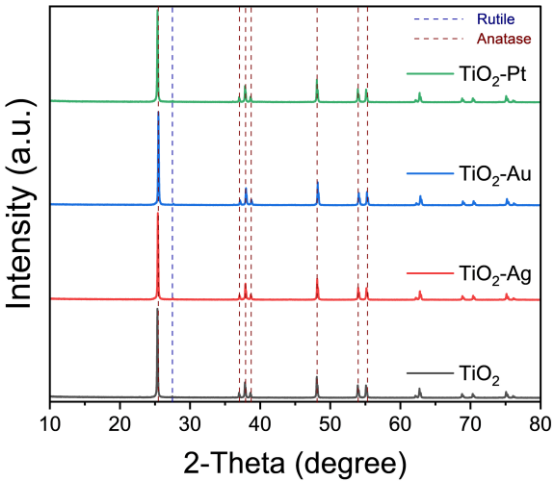


Figure 5 X-ray diffractograms of bare TiO_2 and the three loaded catalysts. Dashed lines mark the reference positions for anatase and rutile.

Every peak belongs to anatase [11], at 25.3°, 37.8°, 48.1°, 53.9°, 55.1°, 62.7°, 68.8°, 70.3° and 75.1°. These are the (101), (004), (200), (105), (211), (204), (116), (220) and (215) planes. Rutile would show at 27.45° and there is nothing above background. The Spurr and Myers method [4] puts rutile at 1.5 wt% everywhere, as little as it can detect. On that evidence the support is pure anatase.

Table 2 Position and width of the anatase (101) reflection, with rutile content from the Spurr and Myers relation.

Sample	2θ (101)	FWHM	Rutile content
Bare TiO_2	25.318°	0.1464°	1.4%
TiO_2/Pt	25.312°	0.1438°	1.6%
TiO_2/Au	25.328°	0.1418°	1.7%
TiO_2/Ag	25.319°	0.1555°	1.5%

The (101) positions agree to 0.016° and the widths to 0.014°, so loading changes neither the lattice nor the crystallite size. Those peaks are narrow and close to the instrument resolution, so Scherrer [5] gives only a lower bound. No gold, silver or platinum peak appears at any (111), (200) or (220) position. At 1 wt% the loading is below what the technique can see, and particles a few nanometres across do not diffract coherently.

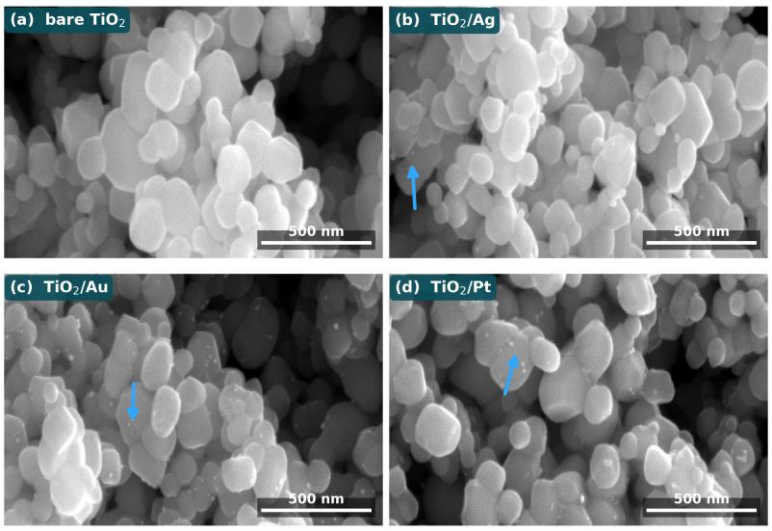


Figure 6 Scanning electron micrographs at matched magnification: (a) bare TiO_2, (b) TiO_2/Ag, (c) TiO_2/Au, (d) TiO_2/Pt. Recorded at 10 kV, 100 pA and 5 µs dwell. Arrows mark metal on the oxide surface. Scale bars 500 nm.

All four show rounded faceted grains of similar size in a loose aggregate. Photodeposition causes no coarsening or sintering, which is what the unchanged line widths would predict. No separate population of metal particles is resolved, which bounds their size and confirms good dispersion.

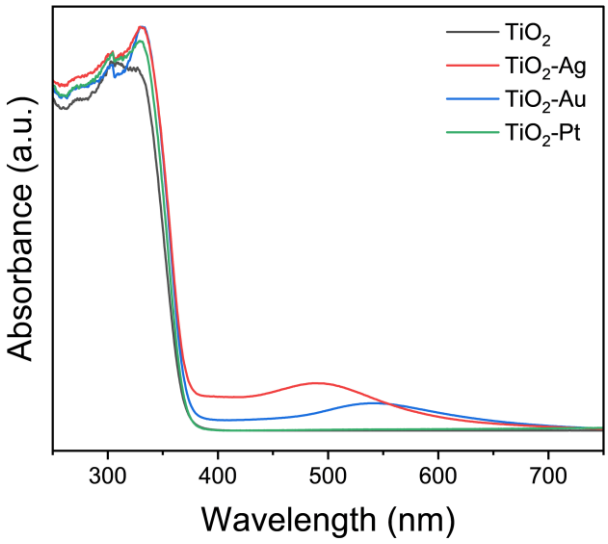


Figure 7 Ultraviolet and visible diffuse reflectance spectra of the four catalysts.

Absorption was measured by diffuse reflectance from 200 to 800 nm. The instrument records absorbance A, so reflectance was recovered as $R = 10^{-A}$ and converted to the Kubelka and Munk function $F(R) = (1-R)^2/2R$ [6]. Anatase has an indirect gap, so the Tauc analysis uses the exponent one half [7]. Points where reflectance falls below 1% were dropped, because the transform amplifies noise there, and the sub-gap baseline from plasmon and scattering was subtracted before fitting.

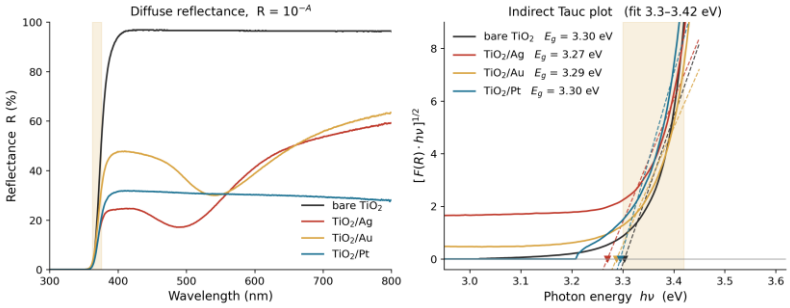


Figure 8 Left: reflectance recovered from the absorbance data. Right: indirect Tauc plot with linear extrapolation to the energy axis. The shaded band marks the common fit window.

Table 3 Indirect band gaps from Kubelka and Munk Tauc analysis, fitted over a common window of 3.30 to 3.42 eV with reflectance restricted to values above 1%.

Sample	Band gap	Absorption edge	Fit quality R^2
Bare TiO_2	3.30 eV	375 nm	0.888
TiO_2/Ag	3.27 eV	379 nm	0.914
TiO_2/Au	3.29 eV	377 nm	0.925
TiO_2/Pt	3.30 eV	376 nm	0.913

Bare TiO_2 absorbs sharply below 380 nm and hardly at all across the visible, as a white powder should. The loaded samples keep that edge and gain absorption at longer wavelengths. Silver and gold show plasmon resonance, silver between 450 and 550 nm peaking near 500 nm, gold between 530 and 570 nm peaking near 550 nm. These bands are the optical signature of metallic nanoparticles, and give the evidence on oxidation state that diffraction cannot.

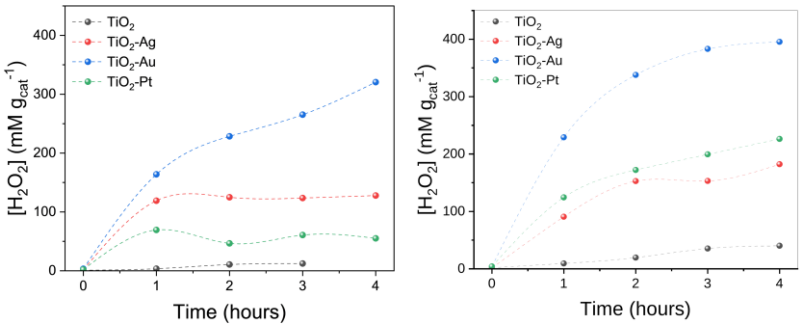


Figure 9 H_2O_2 accumulation over four hours. Left: Regime A, oxygen pre-purge for 30 min at 100 mL per minute with no further supply. Right: Regime B, continuous oxygen purging at 50 mL per minute.

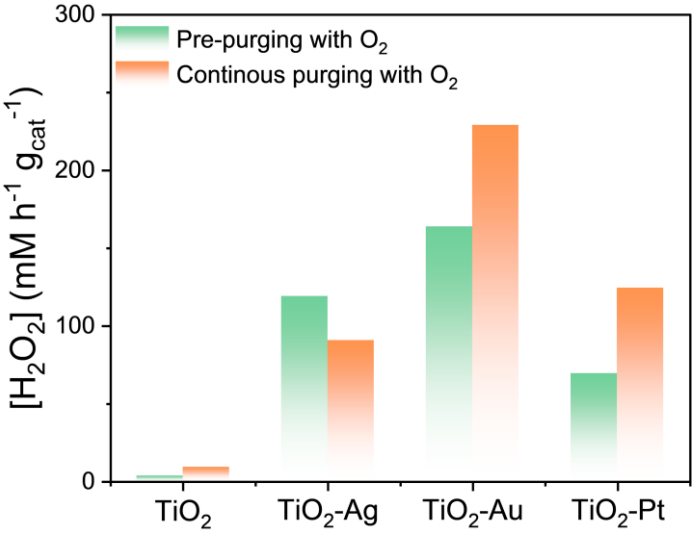


Figure 10 Hydrogen peroxide produced by the four catalysts during the first hour of irradiation. Table 4 lists the same values.

Table 4 Production rates over the first hour of irradiation, in mM h^{-1} g^{-1}, with 10 mg catalyst in 25 mL of 10 vol% aqueous methanol. Values are read from Figure 10 and are quoted to the precision that figure supports. Bare TiO_2 is the baseline.

Catalyst	Regime A	Regime B	Change
Bare TiO_2 (baseline)	2	6	up 200%
TiO_2/Ag	118	88	down 25%
TiO_2/Pt	68	122	up 79%
TiO_2/Au	162	228	up 41%

The four gaps agree to 0.03 eV, so loading does not change the band structure and the extra visible absorption comes from the metal. Absolute values depend on the fit window: shifting it to 3.42 to 3.52 eV raises all four to 3.38 eV. Differences between samples stay below 0.03 eV in every window tested, which is why the window is quoted alongside the values.

5 Discussion

Platinum has the higher work function and traps electrons better, yet gold wins. What matters is what happens after the peroxide forms. Platinum decomposes and further reduces it, so a platinum surface destroys part of what it makes, while gold is comparatively inert. The measurement is formation minus destruction, and gold wins that balance.

How each catalyst responds to the oxygen change says more than the ranking. Bare TiO_2 triples, platinum gains 79% and gold 41%, while silver falls by 25%. The pattern follows how fast each catalyst pulls oxygen out of solution. Under a fixed inventory the faster catalysts use it quicker than

diffusion replaces it, so mass transport rather than photochemistry sets what is measured. Continuous purging lifts that limit.

Silver is the exception, and the flow rates explain it. The pre-purge runs at 100 mL per minute for 30 minutes, so the solution starts richer in oxygen than a 50 mL per minute flow can sustain. Silver draws on that reserve in the first hour and leads, then falls behind once it runs down. Over four hours continuous purging is ahead by 43%, which was not expected from the first hour alone and is the clearest sign that a single early reading can mislead.

The three characterisation techniques agree with each other. Loading leaves the lattice, crystallite size and morphology alone, and the band gap moves by no more than 0.03 eV. Whatever causes the differences in behaviour, it is not a change in the support. Diffraction finds no metal phase, which fits a loading below the detection limit and particles too small to diffract, while the plasmon bands show metallic silver and gold are present. Together these mean the metals sit as well dispersed nanoparticles rather than agglomerates, which is what determines how many active junctions each gram provides.

For platinum and for the bare oxide, better gas-liquid contacting, agitation or pressure would raise the rate more than further work on charge separation. Gold gains least from extra oxygen, so for gold the reverse holds.

6 Limitations and Future Work

- Three concentration readings sit above the assay ceiling of 2000 µM and were obtained by extrapolation: TiO_2/Pt under Regime B at 2263 µM, and TiO_2/Au at 3205 and 4000 µM. Next step: re-assay those three at a higher dilution so every value falls inside the calibrated range.
- The values in Table 4 are read from a bar chart rather than taken from the underlying data, so they carry a wider margin than the four significant figures the spreadsheet holds. Next step: tabulate the first-hour concentrations directly.
- Apparent quantum yield cannot be reported, because the lamp is characterised only by its drive current. Next step: measure the incident photon flux with a calibrated radiometer.
- Metal loading is nominal. Neither diffraction nor microscopy confirms that 1 wt% was achieved or that it is comparable across the three samples. Next step: elemental analysis by ICP-OES.
- Particle size and oxidation state of the deposits are inferred rather than measured. Next step: transmission electron microscopy for size, and X-ray photoelectron spectroscopy for oxidation state.
- Only one loading and one support have been tested. Promising extensions are a loading series to find the optimum, and a support with a narrower band gap so that visible light can be used.

7 Conclusion

Photocatalysis is a workable alternative to the anthraquinone process: a catalyst, light and oxygen replace a multi-step energy-intensive route with a large waste stream, and the product is made where it is used. Gold is the strongest of the three metals under both oxygen regimes. In the first hour under continuous purging it reaches 228 mM h^{-1} g^{-1}, against 6 for the bare oxide. It beats platinum despite the less favourable junction, because platinum decomposes the peroxide it makes. Photodeposition leaves the support unchanged in structure, crystallite size, morphology and band gap, and the plasmon bands show the metal is present as well dispersed nanoparticles. For most of the series the rate is set by the supply of dissolved oxygen rather than by charge separation. That is what the two-regime design was built to expose, and it tells you where further effort belongs for each material. The main takeaway is that TiO_2/Au is the catalyst worth pursuing, and that for the rest of the series reactor engineering will pay off sooner than materials modification.

References

[1] Fujishima, A.; Honda, K. Electrochemical Photolysis of Water at a Semiconductor Electrode. Nature 1972, 238, 37-38.

[2] Campos-Martin, J. M.; Blanco-Brieva, G.; Fierro, J. L. G. Hydrogen Peroxide Synthesis: An Outlook beyond the Anthraquinone Process. Angewandte Chemie International Edition 2006, 45, 6962-6984.

[3] Hou, H.; Zeng, X.; Zhang, X. Production of Hydrogen Peroxide by Photocatalytic Processes. Angewandte Chemie International Edition 2020, 59, 17356-17376.

[4] Spurr, R. A.; Myers, H. Quantitative Analysis of Anatase and Rutile Mixtures with an X-Ray Diffractometer. Analytical Chemistry 1957, 29, 760-762.

[5] Scherrer, P. Bestimmung der Größe und der inneren Struktur von Kolloidteilchen mittels Röntgenstrahlen. Nachrichten von der Gesellschaft der Wissenschaften zu Göttingen 1918, 26, 98-100.

[6] Kubelka, P.; Munk, F. Ein Beitrag zur Optik der Farbanstriche. Zeitschrift für Technische Physik 1931, 12, 593-601.

[7] Tauc, J.; Grigorovici, R.; Vancu, A. Optical Properties and Electronic Structure of Amorphous Germanium. Physica Status Solidi B 1966, 15, 627-637.

[8] Linsebigler, A. L.; Lu, G.; Yates, J. T. Photocatalysis on TiO_2 Surfaces: Principles, Mechanisms, and Selected Results. Chemical Reviews 1995, 95, 735-758.

[9] Kormann, C.; Bahnemann, D. W.; Hoffmann, M. R. Photocatalytic Production of Hydrogen Peroxides and Organic Peroxides in Aqueous Suspensions of Titanium Dioxide, Zinc Oxide, and Desert Sand. Environmental Science and Technology 1988, 22, 798-806.

[10] Shiraishi, Y.; Kanazawa, S.; Sugano, Y.; Tsukamoto, D.; Sakamoto, H.; Ichikawa, S.; Hirai, T. Highly Selective Production of Hydrogen Peroxide on Graphitic Carbon Nitride Photocatalysts Activated by Aromatic Groups. ACS Catalysis 2014, 4, 774-780.

[11] JCPDS Powder Diffraction File 21-1272, Anatase TiO_2. International Centre for Diffraction Data.